DOI: 10.1002/ejic.200600099

Synthesis, Electrochemical and Electrogenerated Chemiluminescence Studies of Ruthenium(II) Bis(2,2′-bipyridyl){2-(4-methylpyridin-2-yl)benzo[*d*]-X-azole} Complexes

Roberto Gobetto,*[a] Giuseppe Caputo,[b] Claudio Garino,[a] Simona Ghiani,[a] Carlo Nervi,[a] Luca Salassa,[a,c] Edward Rosenberg,*[c] J. B. Alexander Ross,[c] Guido Viscardi,[d] Gianmario Martra,[b] Ivana Miletto,[d] and Marco Milanesio[e]

Keywords: Electrochemistry / Luminescence / Ruthenium / ECL / Bioinorganic chemistry

A series of photoactive complexes of [Ru^{II}bis(bipyridyl){2-(4-methylpyridin-2-yl)benzo[*d*]-X-azole}]$(PF_6)_2$ (X = N–CH_3, **1**; S, **2**; or O, **3**) have been synthesized and fully characterized by proton and ^{13}C NMR spectroscopy and UV/Vis spectroscopy. The X-ray structure of **1** is also reported. The electrochemical behavior and the photophysical properties of **1**–**3** have been investigated. Cyclic voltammetry (CV) reveals the presence of three consecutive one-electron reduction processes and a single one-electron oxidation process that are chemically and electrochemically reversible. In all cases, electrogenerated chemiluminescence (ECL) has been observed in the presence of the co-reactant tri-*n*-propylamine (TPA). An analogue of **1** has been synthesized, [Ru^{II}bis(bipyridyl){2-(4-methylpyridin-2-yl)benzo[*d*]-X-azole}]$(PF_6)_2$ [X = $N(CH_2)_5CO_2H$, **4**], it has been coupled with bovine serum albumin (BSA), and its photophysical properties investigated.

Introduction

Luminescent techniques are among the fastest-growing analytical tools in life science and analytical chemistry.[1] These techniques are useful because they couple high sensitivity and selectivity with automated monitoring. Furthermore, many parameters can be detected: luminescence intensity, quantum yield, lifetime, luminescence polarization, quenching efficiency, and radiative and nonradiative energy transfer.

In recent years, metal–ligand complexes (MLCs) have gained paramount importance in luminescence spectroscopy because of their wide range of absorption and emission wavelengths and their long decay times, which range from 100 ns to 10 μs.[1] Careful selection of metal and ligand can result in properties that are helpful for specific applications; for example, absorption wavelengths between 460 and 700 nm can be obtained using osmium and ruthenium in MLCs. Also, ruthenium complexes have been used as lifetime-based optical sensors for pH,[2,3] potassium,[4] chloride,[5] and carbon dioxide detection.[6] In addition, ruthenium complexes have been developed as luminescent probes for immunoassays.[7–10] Furthermore, the rotation of proteins and other macromolecules can be studied by a combination of polarized emission and time-resolved measurements in the microsecond range. Lastly, the use of ruthenium complexes in place of ethidium bromide in DNA analysis has also been reported.[11] In this application, the probe's luminescence increases when it intercalates into double-stranded DNA. Thus, the spectral and temporal resolution of MLC-based excited-state microscopy can result in increased resolution and probe selectivity for biological applications.

Our focus is the development of novel electrogenerated chemiluminescence (ECL) devices suitable for the detection of different biological analytes of clinical and environmental interest. To this end, we report the synthesis, characterization, redox behavior, and photophysical properties of the series of complexes [Ru^{II}bis(bipyridyl){2-(4-methylpyridin-2-yl)benzo[*d*]-X-azole}]$(PF_6)_2$ (X = N–CH_3, **1**; S, **2**; or O, **3**). The use of [2-(4-methylpyridin-2-yl)-1*H*-benzoimidazole] (X = NH) as a free ligand offers the opportunity to introduce a substituent in the 1*H* position suitable for bioconjugation using standard synthetic organic techniques. As an example of a biological application, we also

[a] Dipartimento di Chimica IFM, MI Center of Excellence, Università di Torino,
Via P. Giuria 7, 10125 Torino, Italy
[b] Dipartimento di Chimica IFM, NIS Center of Excellence, Università di Torino,
Via P. Giuria 7, 10125 Torino, Italy
[c] Department of Chemistry, University of Montana,
Missoula, MT 59812, USA
[d] Dipartimento di Chimica Generale ed Organica Applicata and NIS Centre of Excellence, Università di Torino,
Corso M. D'Azeglio 48, 10125 Torino, Italy
[e] Dipartimento di Scienze e Tecnologie Avanzate, Università del Piemonte Orientale,
"A. Avogadro", Via Bellini 25/G, 15100 Alessandria, Italy
E-mail: roberto.gobetto@unito.it
Supporting information for this article is available on the WWW under http://www.eurjic.org or from the author.

report the synthesis of an analogue of **1** in which the methyl group is substituted by 1-hexanoic acid and the resulting complex, **4**, is bioconjugated to bovine serum albumin (BSA) through an amidic bond. Photophysical investigations show efficient luminescence and ECL properties for all the derivatives. The synthesis of **2** and **3** also allows us to evaluate how the electronic and photophysical properties of the metal complex are affected by subtle alterations in the bidentate heterocyclic ligand.

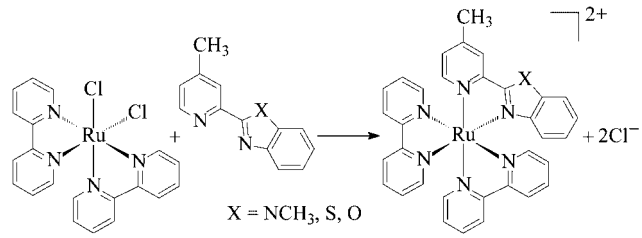

Scheme 1.

Results and Discussion

Following our synthesis of novel metal complexes of ruthenium and osmium with potentially useful fluorescence properties,[12,13] we investigated the reactivity of $Ru(bpy)_2Cl_2$ with bidentate ligands of formula 2-(4-methylpyridin-2-yl)benzo[*d*]-X-azole (X = N–CH_3, S, or O). The choice of this unsymmetrical bidentate ligand, which has a single, easily modifiable site in the case of the benzimidazole ligand, avoids the formation of unwanted isomeric species, which are often difficult to separate from the desired product.

The reaction of $Ru(bpy)_2Cl_2$ with 2-(4-methylpyridin-2-yl)benzo[*d*]-X-azole (X = N–CH_3, S, or O) in refluxing ethylene glycol gives a single orange crystalline product in good yield for all the ligands that have been identified as **1**, **2**, and **3** respectively (Scheme 1). The products have been recrystallized as PF_6^- salts and in the case of **1**, analyzed by single-crystal X-ray diffraction.

Crystal Structure of [Ru^{II}bis(bipyridyl){2-(4-methylpyridin-2-yl)benzo[*d*]-X-azole}]$(PF_6)_2$ (X = N–CH_3, 1)

The crystal structure of **1** is illustrated in Figure 1, crystallographic data are given in Table 5, and selected distances and angles are given in Table 1. The asymmetric unit of the complex is arranged in the $P2_1/c$ space group. Two PF_6^- anions assure the electrical neutrality of the structure. As already observed in related structures,[13,14] the PF_6^- moieties are rather mobile, as evidenced by their large equivalent atomic displacement parameters (ADP), ranging from 0.090(1) for F(2) to 0.149(2) for F(5). Also the atoms belonging to the bpy and 2-pyridyl-benzimidazole ligands show large ADP values. The magnitudes of the ADP increase with increasing distance from the ruthenium atom, as expected. For example, the 6 N atoms, N(1)–N(6), bonded to Ru show ADP values in the range 0.044(1)–0.048(1), whereas C(33), the atom furthest away from the Ru atom, has an ADP value of 0.114(3).

The geometry around the Ru atom is a fairly regular octahedron with five-membered chelate rings having bite

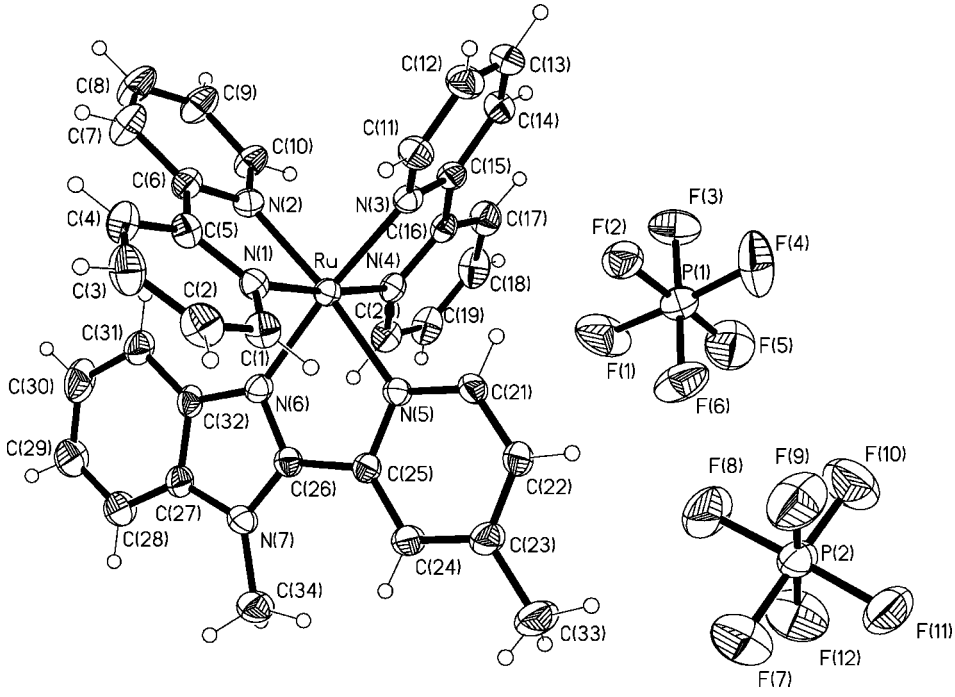

Figure 1. Molecular structure of compound **1** showing the adopted labeling scheme, with displacement ellipsoids drawn at 20% probability. A half-populated CH_3CN moiety, located in the electron density, is not shown for the sake of clarity.

Table 1. Selected distances and bond angles for **1**.[a]

Distances [Å]					
Ru–N(1)	2.051(4)	N(6)–C(32)	1.399(6)	N(1)–C(5)	1.357(6)
Ru–N(2)	2.050(4)	N(6)–C(26)	1.335(5)	N(2)–C(6)	1.349(6)
Ru–N(3)	2.066(4)	C(25)–C(26)	1.469(6)	N(2)–C(10)	1.353(6)
Ru–N(4)	2.064(4)	N(5)–C(25)	1.364(6)	N(7)–C(26)	1.356(6)
Ru–N(5)	2.078(4)	N(5)–C(21)	1.343(6)	N(7)–C(27)	1.395(6)
Ru–N(6)	2.060(4)	N(1)–C(1)	1.324(6)		
Angles [°]					
N(1)–Ru–N(2)	78.9(2)	N(1)–Ru–N(4)	174.3(1)	N(1)–Ru–N(3)	97.6(2)
N(3)–Ru–N(4)	78.9(2)	N(2)–Ru–N(5)	173.0(1)	N(1)–Ru–N(5)	95.6(2)
N(5)–Ru–N(6)	77.4(1)	N(3)–Ru–N(6)	173.3(2)	N(2)–Ru–N(4)	96.3(2)
N(1)–Ru–N(6)	88.5(2)	C(26)–N(6)–C(32)	105.4(4)	N(3)–Ru–N(5)	99.1(1)
N(2)–Ru–N(3)	85.9(2)	C(21)–N(5)–C(25)	116.9(4)	N(4)–Ru–N(6)	95.3(2)
N(4)–Ru–N(5)	89.4(1)	C(6)–N(2)–C(10)	116.8(4)		

[a] Numbers in parentheses are estimated standard deviations.

angles of 78.8(2)°, and the angles between the chelate rings are divided into the usual two groups of 85.9–88.5(2)° and 95.6–99.1(2)° (Table 1). This geometry is very similar to the closely related complex $[Ru(bpy)_2(bbbpyH_2)](ClO_4)_2$ [$bbbpyH_2$ = 2,2′-bis(benzimidazol-2-yl)-4,4′-bipyridine][15] and to bis(bipyridyl) complexes in general.[16,17] Similarly, the Ru–N bipyridyl bond lengths [2.050–2.078(4) Å] and the benzimidazole bond length [Ru–N(6) = 2.060(4) Å] are very similar to Ru–N bonds in the related complexes.[16,17] The N(6)–C(32) and N(6)–C(26) bond lengths of 1.399(6) and 1.335(5) Å are also similar to the previously reported Ru-benzimidazole complex [1.39(1) and 1.35(1) Å] as are the other N–C bonds within the bipyridyl rings.[15] Although it is dangerous to draw conclusions about relative bond strengths from metal–ligand bond lengths alone, it would seem from these data that the benzimidazole ring has donor properties similar to those of the pyridinyl ligands and that these properties are relatively insensitive to substitution of a methyl group in the 3-position of the ring.

In the solid state, the cationic and anionic moieties are vertically stacked in layers (Figure 2), and are stabilized by ionic interactions between anions and cations and by weak C–H···F interactions (dotted lines in Figure 2). The layers are connected by PF_6^- ions to form a low-density structure – 1.570 Mg/m^3 is small for a Ru-containing compound – with channels containing two acetonitrile molecules in half-occupancy. The acetonitrile positions are represented in Figure 2 by circles located in the acetonitrile centers of mass. The acetonitrile molecules are only weakly bound to the cation–anion couple by weak CH···F and CH···N interactions, depicted by broken lines in Figure 3. The geometric features of the C(36)–H···F and C–H···N(8) interactions that are shorter than 3.0 Å are reported in Table 2. The contact distances are large, being just within twice the standard deviation of the sum of the van der Waals radii ($vdW_N + vdW_H$ = 2.75 Å, $vdW_F + vdW_H$ = 2.64 Å) except in the case of the C(36)–H(36B)···F8 contact. Because of the long contact distances, the acetonitrile moiety can be accommodated by optimizing the contact angles, which range from 124(1)° to 154(1)°. The acetonitrile moieties thus have considerable freedom of movement and, in fact, they are disordered in the crystal structure and can be successfully refined only by imposing a 1/2 population of the N(8), C(1), and C(2) atoms.

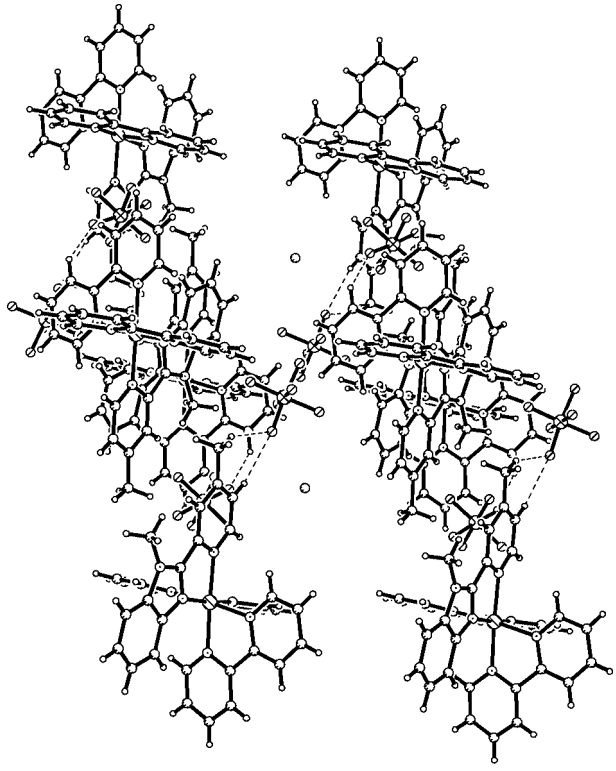

Figure 2. Crystal packing of compound **1**, showing the channels between the layers formed by the $[Ru(bpy)_2(LegN)](PF_6)_2$ ionic couples. Acetonitrile positions are indicated by their center of mass.

NMR Spectroscopy

The ^1H NMR spectrum (Figure 4, top) of **1** recorded in acetone is entirely consistent with the structure found in the solid state, showing 22 proton resonances in the aromatic region from 7.10 to 8.82 ppm and one at δ = 5.94 ppm. Sixteen signals belong to protons of the two-bpy moieties and the other seven are assigned to the 2-(4-methylpyridin-

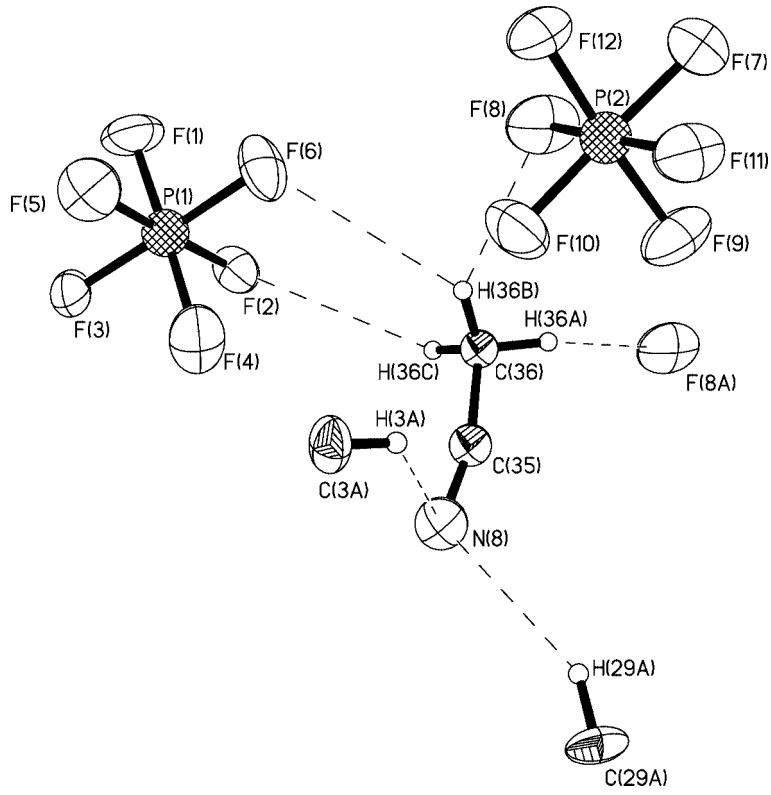

Figure 3. The weak interactions, observed in the solid state, between the acetonitrile moiety and the ions of **1**.

Table 2. Geometric features of the weak hydrogen bonds connecting the acetonitrile moiety and **1** (distances in Å and angles in °).[a]

Compound	**1**
N(8)···H(3A)	2.89(2)
N(8)···H(3A)–C(3A)	135(1)
N(8)···H(29A)	2.72(2)
N(8)···H(29A)–C(29A)	154(1)
H(36A)···F(8A)	2.84(2)
C(36–36A)···F(8A)	147(1)
H(36B)···F(8)	2.54(2)
C(36)–H(36B)···F(8)	144(1)
H(36B)···F(6)	2.98(2)
C(36)–H(36B)···F(6)	133(1)
C(36)–H(36C)···F(2)	2.82(2)
C(36)–H(36C)···F(2)	124(1)

[a] Numbers in parentheses are estimated standard deviations.

2-yl)-benzimidazole ligand. Furthermore, two other signals are observed at δ = 4.5 and 2.5 ppm, assigned to methyl groups of the benzimidazole and pyridine rings, respectively.

As for **1**, the spectra of **2** and **3** also show 23 proton resonances in the aromatic range and a signal at 2.6 ppm because of the 4-pyridine methyl group. The ^{13}C spectra of complexes **1**–**3** are also consistent with the proposed structures (see Figure 4, bottom for **1**).

Electrochemistry

The cyclic voltammetric (CV) response in acetonitrile at a glassy carbon (GC) electrode for each of the Ru derivatives shows three sequential ligand-centered one-electron reductions (Figure 5, top) and a single metal-centered one-electron oxidation (Figure 5, bottom). The electrochemical behavior described is similar to that of the well-known $Ru(bpy)_3Cl_2$ and related complexes.[18] In the particular case of $Ru(bpy)_3Cl_2$, however, the chlorine ions undergo an additional irreversible oxidation in acetonitrile solutions.[19] We do not observe this particular oxidation process in the CV of complexes **1**–**3**, as the counterion is PF_6^-. The redox processes are chemically and electrochemically reversible, with $i_p^a/i_p^c \approx 1$ and $|E_p^c - E_p^a| \approx 60$–70 mV at scan rates ranging from 0.050 to 1.000 V/s. The half-wave redox potentials evaluated as a mean of the cyclic voltammetric anodic and cathodic peaks, as well as the peak-to-peak separations, are reported in Table 3. In the case of **1**, the processes centered at $E_{1/2}(+2/+3)$ = +0.732, $E_{1/2}(+2/+1)$ = –1.782, $E_{1/2}(+1/0)$ = –1.982, and $E_{1/2}(0/-1)$ = –2.215 V versus Fc/Fc^+ are shifted towards more negative values of about 0.2 V when compared with the corresponding values of **2** and **3**. This is in line with the better σ-donor electronic properties of the ligand containing nitrogen. In addition, the closely related mononuclear and dinuclear $Ru(bpy)_2$ complexes of the free ligand 2,2′-bis(benzimidazol-2yl)-4,4′-bipyridine have similar oxidation and reduction potentials.[15,20] The oxidation of $[Ru(bpy)_3]^{2+}$ is at the somewhat more positive potential [$E_{1/2}(+2/+3)$ = +0.881 vs. Fc/Fc^+] in acetonitrile, indicating that the benzimidazole ring is a slightly better donor than bipyridyl. On the contrary, reductions of compounds **2** and **3** occur at less negative potentials. The diffusion coefficient of **1** (D_1) relative to that

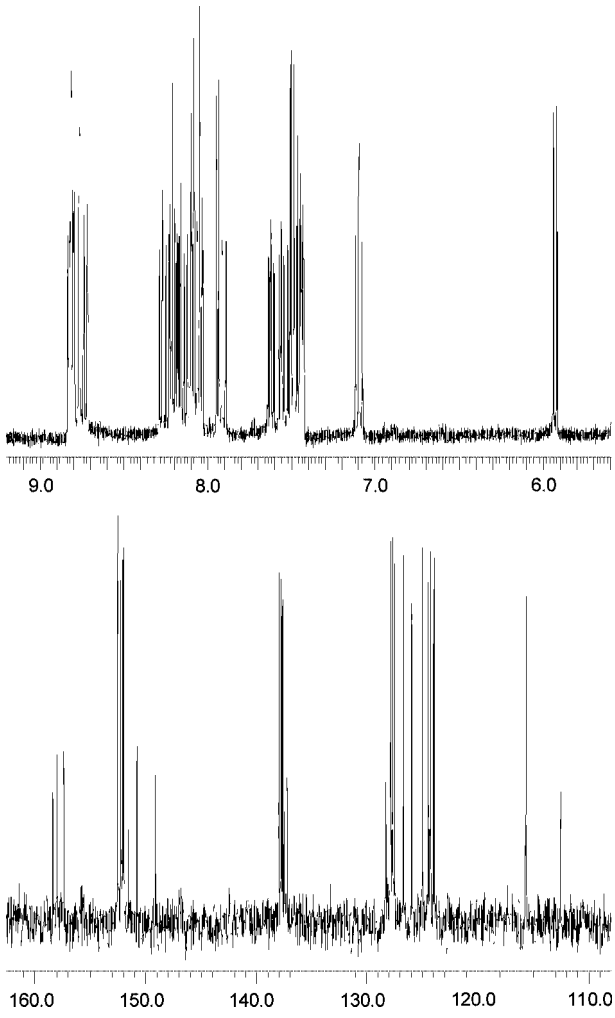

Figure 4. ^{1}H NMR expansion of the aromatic region and ^{13}C NMR of **1** at 400 MHz in acetone.

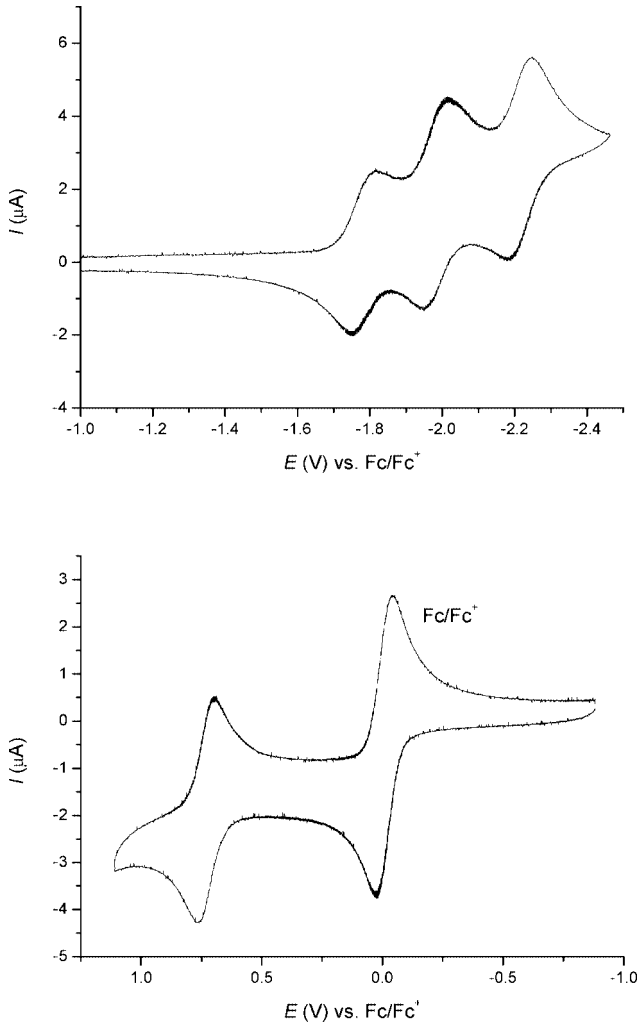

Figure 5. Top: cyclic voltammogram (reduction only) of a 1 mM solution of **1** in MeCN at a GC electrode, scan rate of 0.100 V/s. Bottom: cyclic voltammogram (oxidation only) of an equimolar (1 mM) solution of **1** and ferrocene in MeCN at a GC electrode, scan rate of 0.100 V/s.

of ferrocene (D_{Fc}) can be evaluated to be $D_{\mathbf{1}}/D_{Fc} = 0.588$ through the Nicholson–Shain equation[21] by means of the ratio between the anodic peak current of ferrocene and that of **1** (Figure 5, bottom) because the one-electron oxidation processes are Nernstian. Exactly the same value is obtained[22] by the Stoke–Einstein equation[23] using the crystallographic molecular volumes of **1** and ferrocene:[24]

$D_{\mathbf{1}}/D_{Fc} = (V_{Fc}/V_{\mathbf{1}})^{1/3} = (203.08\ Å^3/1001.5\ Å^3) \approx 0.587$

Absorption Spectra and Photoluminescence

UV/Vis absorption spectra of **1**–**3** are characterized by several ligand-based transitions in the UV with metal-to-ligand charge transfer (MLCT) bands in the visible region. In CH_3CN solution, the complexes display four absorption bands, three in the range of 250–400 nm attributable to the π-to-π* transitions of the bipyridine and heterocyclic rings and one in the 450–460 nm range assigned to a MLCT transition. The MLCT absorption bands display a maximum at 460 nm for **1** and at 450 nm for **2** and **3**. Their luminescent behavior has been investigated by acquiring emission spectra and by evaluating the molar extinction coefficient for absorption and the quantum yields of the emission after irradiation at λ_{max} for the MLCT transition (Table 4).

Table 3. Redox potentials (V vs. Fc/Fc^+) and peak-to-peak separation in parenthesis (mV) at a scan rate of 0.1 V/s in acetonitrile for the reference $Ru(bpy)_3Cl_2$ and complexes **1**–**3**.

$E_{1/2}$	$Ru(bpy)_3Cl_2$	**1**	**2**	**3**
+2/+3	+0.881 (70)	+0.732 (65)	+0.920 (86)	+0.944 (77)
+2/+1	–1.738 (66)	–1.782 (66)	–1.506 (75)	–1.579 (70)
+1/0	–1.923 (69)	–1.982 (71)	–1.886 (77)	–1.898 (73)
0/–1	–2.165 (75)	–2.215 (66)	–2.138 (82)	–2.145 (85)
–1/–2	–2.77 (irr)	–2.72 (irr)	–2.560 (72)	–2.63 (irr)
–2/–3		–2.91 (irr)	–2.98 (irr)	–2.89 (irr)

The systems display broad emission spectra with maximums in energy at 634, 684, and 666 nm with Stoke's shifts of 174, 234, and 216 nm for **1**–**3**, respectively. Quantum efficiencies were found to be 0.021, 0.008, and 0.008 for **1**–**3**, respectively. These values were determined using $Ru(bpy_3)^{2+}$ ($\Phi_{em} = 0.062$)[25] as a standard (Table 4). The lumi-

Table 4. MLCT absorptions, extinction coefficient, emission properties, and ECL efficiencies for **1**–**3**.

	λ_{ex} (nm)	ε	λ_{em} (nm)	Φ_{em}	δ (nm)	τ (ns)	Φ_{ECL}
$Ru(bpy)_3^{2+}$	450	13300	614	0.062	164	890	1
1	460	12200	634	0.021	174	139	0.35
2	450	10700	684	0.008	234	184	0.04
3	450	10700	666	0.008	216	138	0.03

nescence lifetimes of the metal complexes, determined by time-correlated single-photon counting as described in Methods, were single exponential decays (see Table 4).

Electrogenerated Chemiluminescence

Electrochemiluminescence (ECL) involves the production of reactive intermediates at the electrode surface from stable precursors. These intermediates can react in various ways to form excited states that emit light at or near the electrode surfaces. ECL has useful commercial applications in clinical analyses (e.g. immunoassays, DNA probes) using $Ru(bpy)_3^{2+}$ and a co-reactant to generate the signal. The co-reactant is generally defined as a species that, after electrochemical oxidation or reduction, produces intermediates that can react with other compounds in the solution and that are able to produce excited states. We used the well-known tri-*n*-propylamine (TPA) as co-reactant. Details of the mechanism by which TPA acts[26] are found in the excellent ECL review by Richter.[27] Compounds **1**–**3** show stable reversible electrochemistry, and therefore are promising ECL luminophores.

Solutions containing only the Ru complex or only the co-reactant do not give an ECL signal. The intense ECL signals resulting from the oxidation of TPA in aqueous solutions of all three complexes were acquired simultaneously with the CV in the potential range between 0 and +1.5 V, at a scan rate of 50 mV/s. The ECL efficiencies, Φ_{ECL}, in water were estimated using the following equation:[28,29]

$$\Phi_{ECL} = \Phi°_{ECL}(IQ°/I°Q)$$

where $\Phi°_{ECL}$ is the ECL efficiency of the standard $Ru(bpy)_3Cl_2$ under the same conditions, I and $I°$ are the integrated ECL intensities of the luminophore under investigation, and the standard, and Q and $Q°$ are the charges passed (in coulombs) for the luminophore and the standard, respectively. In experiments performed with the co-reactant, the absolute ECL quantum efficiency for the reference system $Ru(bpy)_3Cl_2$/TPA is unknown, so relative efficiencies are reported taking its $\Phi°_{ECL} = 1$. The Φ_{ECL} values in Table 4 are a mean of the first three sequential measurements and are subject to an error of about ±10%. It has been reported that adsorption phenomena could influence the ECL emission.[30,31] Moreover, the MLCT states, and hence the luminescence properties, are sensitive to the nature of the environment and to the solvation shell.[32] Typical ECL responses are sketched in Figure 6.

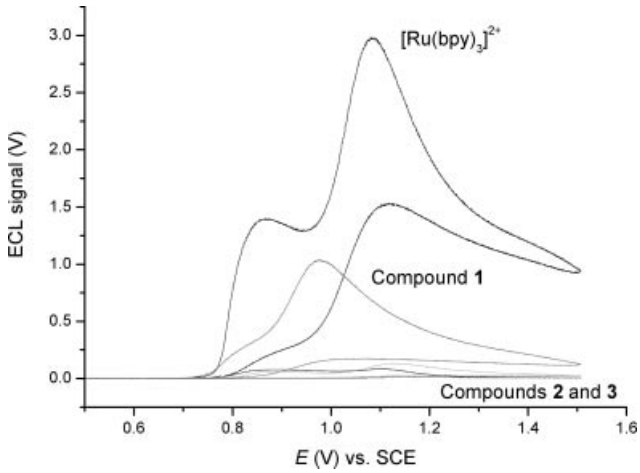

Figure 6. Electrochemiluminescence (ECL) of complexes **1**–**3** in the presence of tri-*n*-propylamine (TPA) in water borate buffer at pH = 8.5.

The presence of dissolved oxygen in water (acquired primarily from ambient air) is undesirable, as this often results in quenching of the luminophore. However, at the high TPA concentrations used in this work (20 mM), the influence of dissolved oxygen on the emission of the $Ru(bpy)_3^{2+}$/TPA system is negligible, provided the source of oxygen is air only.[33] For these reasons we performed all measurements in air.

Despite the limitations described above, it is worth noting that the Φ_{ECL} for **1** is almost an order of magnitude greater than either **2** or **3**. This is undoubtedly due to the lower oxidation potential of **1** relative to **2** and **3**. It is generally accepted that the primary mechanisms for producing ECL with $Ru(bpy)_3^{2+}$ in the presence of the co-reactant TPA are: (1) oxidation of $Ru(bpy)_3^{1+}$, produced by reduction of $Ru(bpy)_3^{2+}$ by $TPA^{\cdot}$ (this species results from ejection of a proton from the relatively long-lived $TPA^{\cdot+}$), which gives rise to an excited state $Ru(bpy)_3^{2+}$; and (2) reduction of electrochemically generated $Ru(bpy)_3^{3+}$ by $TPA^{\cdot}$ to give the same excited state $Ru(bpy)_3^{2+}$.[26] In the ECL spectrum reported in Figure 6, the first peak is due to the effect of the oxidation of TPA at the electrode, whereas the latter is relative to the oxidation of $Ru(bpy)_3^{2+}$.[26] In the case of **1**, its lower oxidation potential relative to **2** and **3** would contribute to both of these mechanisms. The better donor properties of the benzimidazole ligand are not only due to electronegativity considerations, but also to the expected greater contribution of the resonance structure (shown in Scheme 2) as a result of more efficient π overlap.

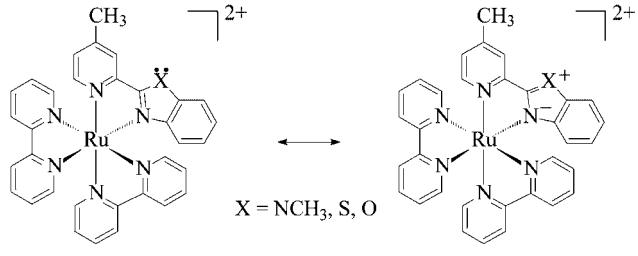

Scheme 2.

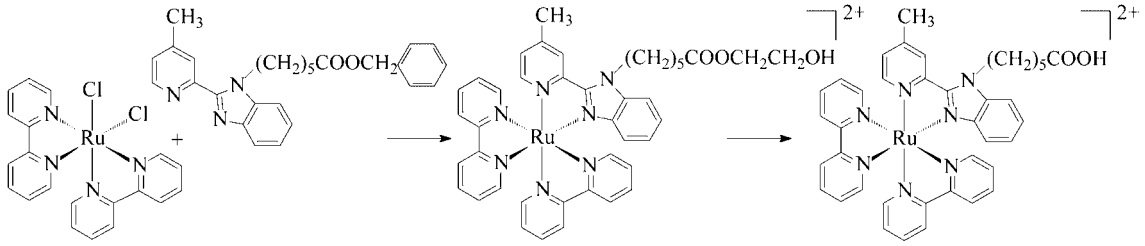

Scheme 3.

Bioconjugation

Although the ECL efficiency of **1** is only about one-third that of $Ru(bpy)_3^{2+}$, its luminescent properties are sufficient to take advantage of the fact that the 2-(4-methylpyridin-2-yl)-benzo-X-azole (X = NH) ligand can be readily and regioselectively modified at the NH group with a linker suitable for bioconjugation. Thus, by reacting $Ru(bpy)_2Cl_2$ with the benzyl ester in ethylene glycol, an intermediate 1-hexanoic acid glycol ester analogue of **1** is obtained, which on acid hydrolysis yields the corresponding hexanoic acid complex **4** in good yield (Scheme 3).

This complex was characterized by one- and two-dimensional ^1H NMR and ^{13}C NMR spectroscopy. Complex **4** has virtually the same absorption spectrum as **1**, showing absorption maxima at 250, 290, 330, and 458 nm and emission band at 630 nm.

The reaction of **4** with *N*-hydroxysuccinimide (NHS) in the presence of dicyclohexylcarbodiimide (DCC) in anhydrous DMF gives the activated succinimide ester **4-NHS** (Scheme 4),[34] suitable for bioconjugation with BSA. The primary structures of BSA, a 67-kDa acidic protein with prolate ellipsoidal shape, and its human homologue, HSA,[35] are well established.[36] Among the 582 amino acids that form BSA, 59 lysines and one N-terminal residue are potentially available for the coupling. In nondenaturing conditions (i.e. low temperature, physiological pH, and low concentration of organic co-solvent), 30–40 lysines are believed to be accessible to coupling reagents.[37] The reaction was monitored by HPLC, and the unstable activated ester **4-NHS** was immediately incubated with BSA in borate buffer (pH = 8.5, ratio dye:protein = 10:1). The resulting **4**-BSA conjugate was purified by gel exclusion chromatography on a Sephadex G-25 M prepacked column with detection at 460 nm. The **4**-BSA conjugate showed an absorption spectrum virtually identical to that of **4** except for increased absorbance at 280 nm because of the protein (Figure 7). Irradiation of the **4**-BSA conjugate at 460 nm gave an emission at 630 nm, identical to that of **4** and very similar to that of **1** (Figure 8). It must be noted that, besides the similarity in shape, the photoluminescent signal of the solution of **4** alone and **4-BSA** equimolar in fluorophore (determined on the basis of the dye-to-protein ratio reported below) exhibited almost the same intensity, indicating that **4** maintains its Φ_{em} when linked to the protein. The dye-to-protein ratio of the **4**-BSA conjugate and the whole protein concentration were estimated by measuring the absorbance of **4-BSA** at 460 nm (ε_{460} = 12200 M^{-1}/cm)[38,39] and by the Bradford method,[40] respectively. The molar dye-to-protein conjugation ratio of **4-BSA** was 1.2.

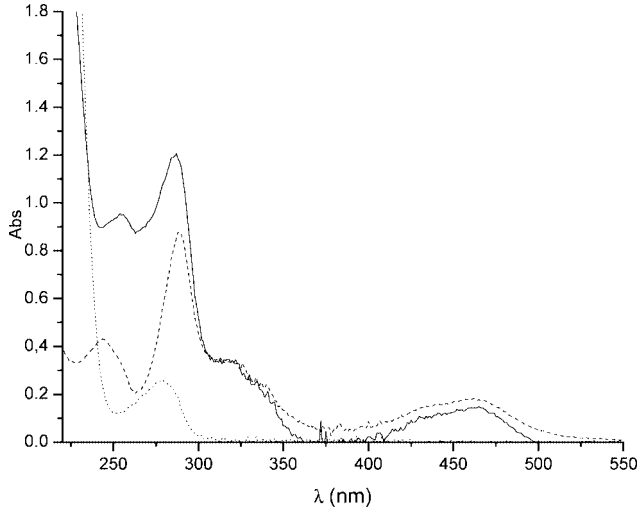

Figure 7. UV/Vis absorption spectra of BSA (···), **4** (----), and **4-BSA** (—) in water borate buffer at pH = 8.5.

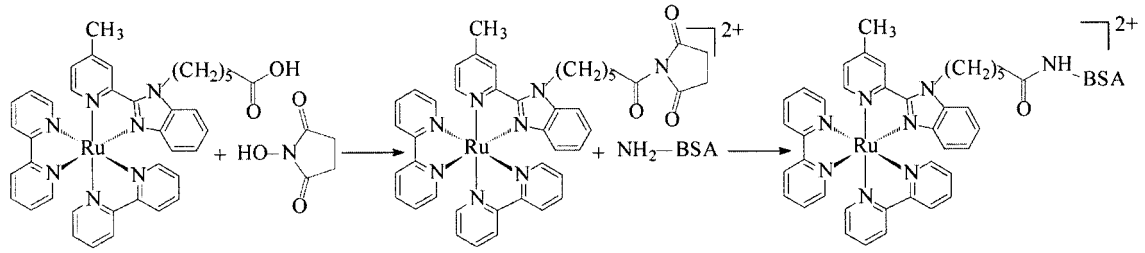

Scheme 4.

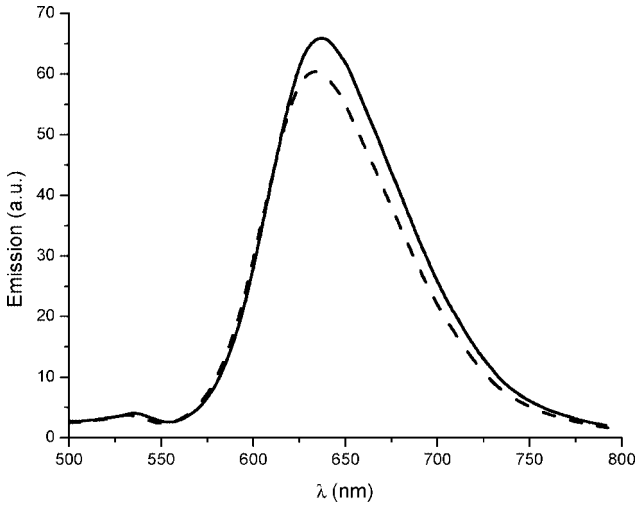

Figure 8. Emission spectra, obtained under irradiation at 460 nm, of **4** (---) and **4-BSA** (—) in water borate buffer at pH = 8.5.

Conclusions

We report a new series of ruthenium complexes based on the ligand system 2-(4-methylpyridin-2-yl)benzo[*d*]-X-azole (X = N–CH_3, S, or O). The benzimidazole complex **1** exhibits the highest quantum yield for luminescence and also the highest ECL efficiency based on its superior donor properties. The X-ray crystal structure of **1** is reported. The photophysical and ECL properties of the series correlate well with their electrochemical properties, and this observation for a homologous series such as **1**–**3** lends support to the idea that such correlations should be general. This study shows also that the ECL emission of **1** in aqueous solutions with the co-reactant TPA is 0.35 times that of the reference compound $Ru(bpy)_3Cl_2$, still reasonably efficient for use as a biological marker. Furthermore, the protocol presented here for bioconjugation is particularly valuable because it provides a simple pathway that can be generalized for linking **4** to small peptides for selective conjugation to proteins and protein receptor sites. The carboxylic acid group in **4** can also be easily modified to target other functionalities besides primary amines.

Further studies are currently in progress for the synthesis of ruthenium derivatives bioconjugated to monoclonal antibodies to serve as novel photoluminescent and electrochemiluminescent probes for diagnostics at very low concentration.

Experimental Section

Materials: Ruthenium(III) chloride hydrate was purchased from Lancaster and used as received. 2,2′-Bipyridine, obtained from Aldrich, was purified by crystallization from hexane and dried under vacuum over P_2O_5.[41] *cis*-$[Ru(bpy)_2Cl_2]\cdot 2H_2O$ was prepared according to the literature methods.[42] The intermediate 6-bromohexanoic acid benzyl ester[43] and the ligands 2-(4-methylpyridin-2-yl)benzo[*d*]-X-azole (X = N–CH_3, S, or O) and 2-(4-methylpyridin-2-yl)-1*H*-benzoimidazole[44,45] were prepared according to published procedures. Tetrabutylammonium hexafluorophosphate ($TBAPF_6$) was obtained as previously reported.[12] Acetonitrile was distilled from calcium hydride just before use. Triple-distilled water was used routinely. BSA was purchased from Fluka and used as received. Prepacked PD-10 columns Sephadex™ G-25 M were purchased from Amersham Biosciences. All other reagents and solvents, obtained from commercial suppliers, were of reagent grade and were used as received without any further purification. All the reactions involving the metal complexes were carried out in argon by standard Schlenk techniques.

Physical Methods: NMR spectra were recorded with a JEOL EX 400 spectrometer (B_0 = 9.8 T, ^1H operating frequency 399.78 MHz) with chemical shifts referenced to residual protons in the solvent ([D_6]acetone). Absorption spectra were measured at room temperature, using a DR LANGE CADAS 200 spectrophotometer, and emission spectra were measured with a Perkin Elmer LS 55 spectrofluorimeter.

Luminescence lifetimes were performed under magic angle polarization conditions by time-correlated single-photon counting[1] using excitation with picosecond pulses of 455-nm light at a repetition rate of 500 kHz generated by a Ti:Sapphire laser system (Verdi V10, Mira 900, and pulse picker from Coherent, Inc., Santa Clara, CA. Second harmonic generation was provided by a 5-050 system from Inrad, Northvale, NJ). The sample was maintained at 20 °C in an automated sample chamber (FLASC 1000 from Quantum Northwest, Spokane, WA). The emission was collected using a bandpass of 20 nm. The data were collected into 2048 channels (1 ns/channel) to 40000 counts in the peak channel. Because the excitation pulse is essentially a delta function at this time resolution, the decays were fit directly without reconvolution as sums of exponentials using Origin 7 (Northampton, MA 01060, USA). IR spectra were recorded with a V22 Bruker FTIR spectrophotometer with a resolution of 2 cm^{-1} and an accumulation of 64 scans.

Electrochemistry: Electrochemistry was performed either with an EG&G PAR 273 electrochemical analyzer or with an AMEL potentiostat model 7050 connected to a PC. All experiments employed a standard three-electrode cell; the reference electrode was a 3 M KCl calomel electrode, the auxiliary electrode a platinum wire, and the working electrode a glassy carbon (GC) with a diameter of 1 mm (CV in acetonitrile) or 2 mm (ECL experiments in water). Positive feedback *iR* compensation was applied routinely. Measurements were carried out either in water or acetonitrile. The supporting electrolytes were 0.1 M phosphate buffer and tetrabutylammonium hexafluorophosphate ($TBAPF_6$), in water and acetonitrile, respectively.

Experiments in acetonitrile were carried out in argon. We used ferrocene (Fc) as an internal standard, and potentials are reported relative to the Fc(0/+1) redox couple [measured $E_{1/2}$(0/+1) = 0.384 V in MeCN, with a peak-to-peak separation of 65 mV]. The aqueous measurements were carried out in air, and the potentials reported relative to the 3 M KCl Calomel Electrode. The ECL along with the cyclic voltammetric (CV) signals (scan rate of 50 mV/s) were measured simultaneously with the AMEL 7050 combined with a photomultiplier tube (PMT, Hamamatsu H9306-03) installed under the electrochemical cell. A home-built power supply (±15 V) regulates the amplification of the PMT, which is directly proportional to the logarithm of the output (between 0 and 10 V). A dark cage, equipped with electrical connection for WE, RE, CE, stirring and inert gas inlet, was built around the electrochemical cell and the PMT, resulting in a background current at the maximum PMT amplification of about 18 ± 12 mV. The measurements were made at half-amplification, where the signal output is attenuated about 200 times with respect to the maximum of the amplifi-

cation. The concentration of the solutions employed were: TPA 20 mM, $Ru(bpy)_2LX$ 1.0×10^{-6} M, supporting electrolyte 0.1 M.

X-ray Structure Determination: The crystal structure of **1** was solved by single-crystal X-ray diffraction analysis. Suitable crystals were obtained by slow evaporation of an acetonitrile–ethanol solution. Diffraction data were collected at room temperature on a Bruker SMART-APEX CCD[46] area detector diffractometer, using graphite monochromated Mo-K_α = 0.71073 Å radiation. Absorption correction was performed using SADABS.[47] The structure was solved by direct methods (SIR97)[48] and refined by full-matrix least-squares (SHELX97).[49] All hydrogen atoms were generated in their calculated positions with the XP[50] software and refined as riding atoms. All non-hydrogen atoms, except C1, C2, and N8 belonging to the acetonitrile molecule, were refined employing anisotropic ADP parameters. Two restraints on the C1–C2 and on the C2–N8 distances were used because of the disorder of the acetonitrile moiety. Crystallographic data and details of data collections and refinements are given in Table 5.

Table 5. Crystal data for **1**.

	1
Empirical formula	$C_{35}H_{30.5}F_{12}N_{7.5}P_2Ru$[a]
Formula weight	947.18
Temperature [K]	293(2)
Wavelength [Å]	0.71069
Crystal system	monoclinic
Space group	$P2_1/c$
a [Å]	13.254(2)
b [Å]	12.129(2)
c [Å]	25.034(5)
α [°]	95.49(3)
V [Å^3]	4005.9(2)
Z	4
Density (calculated) [Mg/m^3]	1.570
Absorption coefficient [mm^{-1}]	0.564
F(000)	1900
Crystal size [mm]	$0.26\times0.24\times0.22$
θ range for data collection [°]	1.54–24.71
Index range	$-15 \le h \le 15$ $-14 \le k \le 14$ $-29 \le l \le 29$
Reflections collected	46984
Independent reflections	6833 [R_{int} = 0.0387]
Completeness to θ = 24.71°	100.0%
Refinement method	full-matrix least-squares on F^2
Data/restraints/parameters	6833/2/512
Goodness-of-fit on F_2	1.007
Final R indices [$I > 2\sigma(I)$]	R_1 = 0.0525, wR_2 = 0.1529
R indices (all data)	R_1 = 0.0681, wR_2 = 0.1587
Largest diff. peak and hole [Å^{-3}]	1.274 and –0.776

[a] The empirical formula has nonintegral values because of the half-populated CH_3CN moiety.

CCDC-288567 contains the supplementary crystallographic data for this paper. These data can be obtained free of charge at www.ccdc.cam.ac.uk/data_request/cif.

Synthesis of Complexes

[Ru(bpy)$_2${1-methyl-2-(4-methylpyridin-2-yl)-1*H*-benzo[*d*]imidazole}](PF$_6$)$_2$ (X = N–CH$_3$, 1): $[Ru(bpy)_2Cl_2]\cdot2H_2O$ (0.200 g, 3.84×10^{-4} mol) and 1-methyl-2-(4-methylpyridin-2-yl)-1*H*-benzo[*d*]imidazole (0.128 g, 5.73×10^{-4} mol) were refluxed in ethylene glycol (50 mL) for 4 h. After cooling to room temperature, water (20 mL) and an aqueous NH_4PF_6 solution (1.0 g/10 mL) were added and the resulting precipitate was collected. The crude product was recrystallized from acetonitrile/ethanol. The sample was dried under vacuum for several hours before elemental analysis. Yield: 0.286 g (80.4%).

$C_{34}H_{29}F_{12}N_7P_2Ru$ (926.65): calcd. (from **1** without crystallization solvent) C 44.07, H 3.15, N 10.58; found C 43.80, H 3.65, N 9.59. ^{1}H NMR (400 MHz, [D$_6$]acetone): δ = 8.82 (m, 3 H), 8.77 (s, 1 H), 8.73 (d, 1 H, J = 8.05 Hz), 8.28 (t of d, 1 H, J_1 = 7.87, J_2 = 1.46 Hz), 8.16 (m, 5 H), 8.05 (t, 2 H, J_1 = 6.04 Hz), 7.95 (d, 1 H, J = 8.86 Hz), 7.91 (d, 1 H, J = 8.54 Hz), 7.63 (m, 1 H), 7.57 (m, 1 H), 7.48 (m, 4 H), 7.10 (t, 1 H, J = 7.81 Hz), 5.94 (d, 1 H, J = 8.42 Hz), 4.59 (s, 3 H), 2.63 (s, 3 H) ppm. ^{13}C NMR (100 MHz, [D$_6$]acetone): δ = 159.92, 159.54, 158.96, 158.92, 154.06, 154.03, 153.77, 153.61, 153.53, 153.09, 152.30, 150.65, 142.24, 139.50, 139.32, 139.18, 139.00, 138.78, 129.85, 129.43, 129.36, 129.22, 129.04, 128.22, 127.50, 126.53, 126.01, 125.85, 125.78, 125.48, 117.19, 114.02, 34.62, 22.00 ppm.

[Ru(bpy)$_2${2-(4-methylpyridin-2-yl)benzo[*d*]thiazole}](PF$_6$)$_2$ (X = S, 2): $[Ru(bpy)_2Cl_2]\cdot2H_2O$ (0.200 g, 3.84×10^{-4} mol) and 2-(4-methylpyridin-2-yl)benzo[*d*]thiazole (0.130 g, 5.74×10^{-4} mol) were refluxed in ethylene glycol (50 mL) for 4 h. After cooling to room temperature, water (20 mL) and an aqueous NH_4PF_6 solution (1.0 g/10 mL) were added and the resulting precipitate was collected. The crude product was washed with water and dried with diethyl ether. Yield: 0.298 g (83.5%). $C_{33}H_{26}F_{12}N_6P_2RuS$ (929.67): calcd. C 42.63, H 2.82, N 9.04; found C 43.47, H 2.93, N 8.77. Deviation of the C% value from the calculated one indicates the presence of some impurity, probably because of the presence of reaction solvent. ^{1}H NMR (400 MHz, [D$_6$]acetone): δ = 8.86 (m, 3 H), 8.76 (d, 1 H, J = 8.05 Hz), 8.67 (s, 1 H), 8.36 (d, 1 H, J = 7.81 Hz), 8.26 (m, 5 H), 8.15 (t of d, 1 H, J_1 = 8.05, J_2 = 1.46 Hz), 8.06 (d, 1 H, J = 4.88 Hz), 8.01 (d, 1 H, J = 5.61 Hz), 7.91 (d, 1 H, J = 5.74 Hz), 7.68 (m, 1 H), 7.63 (m, 1 H), 7.55 (m, 4 H), 7.34 (m, 1 H), 6.48 (d, 1 H, J = 8.54 Hz), 2.62 (s, 3 H) ppm. ^{13}C NMR (100 MHz, [D$_6$]acetone): δ = 168.85, 159.69, 159.34, 158.89, 158.82, 154.68, 154.59, 153.97, 153.68, 153.58, 153.18, 152.91, 140.06, 139.94, 139.72, 139.64, 135.86, 131.16, 130.28, 129.85, 129.68, 129.64, 129.62, 129.55, 129.13, 126.19, 126.14, 126.00, 125.79, 121.40, 21.70 ppm.

[Ru(bpy)$_2${2-(4-methylpyridin-2-yl)benzo[*d*]oxazole}](PF$_6$)$_2$ (X = O, 3): $[Ru(bpy)_2Cl_2]\cdot2H_2O$ (0.200 g, 3.84×10^{-4} mol) and 2-(4-methylpyridin-2-yl)benzo[*d*]oxazole (0.120 g, 5.71×10^{-4} mol) were refluxed in ethylene glycol (50 mL) for 4 h. After cooling to room temperature, water (20 mL) and an aqueous NH_4PF_6 solution (1.0 g/10 mL) were added and the resulting precipitate was collected. The crude product was washed with water and dried with diethyl ether. Yield: 0.275 g (78.4%). $C_{33}H_{26}F_{12}N_6OP_2Ru$ (913.61): calcd. C 43.38, H 2.87, N 9.20; found C 43.84, H 3.04, N 9.04. ^{1}H NMR (400 MHz, [D$_6$]acetone): δ = 8.84 (m, 3 H), 8.76 (d, 1 H, J = 8.18 Hz), 8.53 (s, 1 H), 8.46 (d, 1 H, J = 5.61 Hz), 8.30 (m, 2 H), 8.20 (m, 4 H), 8.08 (d, 1 H, J = 5.61 Hz), 7.98 (s, 1 H), 7.96 (d, 1 H, J = 3.17 Hz), 7.60 (m, 6 H), 7.34 (t, 1 H, J = 7.87 Hz), 6.12 (d, 1 H, J = 8.18 Hz), 2.66 (s, 1 H) ppm. ^{13}C NMR (100 MHz, [D$_6$]-acetone): δ = 165.62, 160.03, 159.62, 158.84, 154.80, 154.49, 154.32, 154.17, 153.86, 153.21, 153.08, 146.94, 140.46, 140.06, 139.66, 132.06, 130.44, 129.75, 129.51, 129.43, 129.16, 128.90, 128.55, 126.11, 125.94, 125.85, 125.63, 118.36, 114.54, 21.82 ppm.

Benzyl 6-[2-(4-Methylpyridin-2-yl)benzoimidazol-1-yl]hexanoate: Freshly sublimated potassium *tert*-butoxide (0.63 g, 5.6×10^{-3} mol) was added to a 50-mL three-neck round-bottom flask containing a solution of 2-(4-methylpyridin-2-yl)-1*H*-benzoimidazole (1 g, 4.80×10^{-3} mol) in anhydrous dimethylformamide (10 mL) at room temperature in argon. After 15 min of mechanical stirring a solu-

tion of 6-bromohexanoic acid benzyl ester (4.6 g, 0.016 mol) in dimethylformamide (2.5 mL) was added drop by drop. After 15 h of heating at 45 °C, the mixture was cooled and deionized water (20 mL) added. The mixture was extracted with ethyl acetate, and the organic layers were dried with anhydrous sodium sulfate, evaporated under vacuum, and purified chromatographically over silica gel with linear gradients using hexane/ethyl acetate mixture as eluent, 95:5 to 70:30. A slightly yellow oil was obtained with a yield of 75% (1.49 g). ^{1}H NMR (400 MHz, CD_2Cl_2): δ = 8.82 (m, 3 H), 8.77 (s, 1 H), 8.50 (d, 1 H, J = 5.00 Hz), 8.23 (s, 1 H), 7.73 (d, 1 H, J = 7.20 Hz), 7.43 (d, 1 H, J = 7.20 Hz), 7.32 (m, 7 H), 7.15 (d, 1 H, J = 5.00 Hz), 5.06 (s, 2 H), 4.80 (t, 2 H, J = 7.57 Hz), 2.43 (s, 3 H), 2.31 (t, 2 H, J = 7.57 Hz), 1.89 (m, 2 H, J = 7.57 Hz), 1.68 (m, 2 H, J = 7.57 Hz), 1.38 (m, 2 H, J = 7.57 Hz) ppm. ^{13}C NMR (100 MHz, CD_2Cl_2): δ = 173.31, 150.82, 150.23, 148.63, 148.30, 143.00, 136.97, 136.64, 128.68, 128.28, 125.45, 124.90, 123.17, 122.40, 120.02, 110.39, 66.14, 45.38, 34.20, 29.83, 26.43, 24.65, 21.08 ppm.

[Ru(bpy)$_2${6-[2-(4-methylpyridin-2-yl)benzo[*d*]imidazol-1-yl]hexanoic acid}](PF$_6$)$_2$ (4): [Ru(bpy)$_2$Cl$_2$]·2H$_2$O (0.200 g, 3.84×10^{-4} mol) and benzyl 6-{2-(4-methylpyridin-2-yl)benzo[*d*]imidazol-1-yl}hexanoate (0.185 g, 5.74×10^{-4} mol) were dissolved in ethylene glycol (50 mL). The mixture was degassed with argon for 15 min and then refluxed for 4 h. After cooling at room temperature, water (20 mL) and an aqueous solution of NH_4PF_6 (1.0 g/10 mL) were added. The precipitate was then collected, washed with water (10 mL) and dried with Et_2O. 0.304 g of [Ru(bpy)$_2${2-(4-methylpyridin-2-yl)-benzo-X-azole}](PF$_6$)$_2$ [X = N(CH$_2$)$_5$CO$_2$CH$_2$CH$_2$OH] was obtained (yield 74%). The complex was dissolved in methanol (80 mL) containing 10% KOH and then stirred for 15 h at room temperature. After acidification at pH ≈ 2–3 with H_2SO_4, the methanol was removed at reduced pressure, and the acidic solution was extracted with dichloromethane. All the organic fractions were collected, dehydrated with Na_2SO_4, and the solvent was removed at reduced pressure. Yield: 0.250 g (86%). ^{1}H NMR (400 MHz, [D$_6$]-acetone): δ = 8.82 (m, 3 H), 8.72 (d, 1 H, J = 8.05 Hz), 8.58 (s, 1 H), 8.27 (t, 1 H, J = 8.05 Hz), 8.19 (m, 3 H), 8.09 (m, 3 H), 8.04 (d, 1 H, J = 5.37 Hz), 7.96 (m, 2 H), 7.63 (t, 1 H, J = 6.35 Hz), 7.52 (m, 4 H), 7.44 (d, 1 H, J = 5.61 Hz), 7.11 (t, 1 H, J = 7.81 Hz), 5.96 (d, 1 H, J = 8.42 Hz), 5.08 (t, 1 H, J = 7.14 Hz), 2.63 (s, 3 H) 2.26 (d, 2 H, J = 7.20 Hz), 2.13 (m, 2 H), 1.65 (m, 2 H), 1.52 (m, 2 H) ppm. ^{13}C NMR (400 MHz, [D$_6$]acetone): δ = 175.21, 159.86, 159.44, 158.94, 158.91, 153.92, 153.88, 153.49, 153.42, 152.52, 152.22, 150.24, 142.27, 139.54, 139.36, 139.25, 139.06, 138.48, 129.92, 129.46, 129.41, 129.31, 129.04, 127.90, 127.72, 126.73, 126.05, 125.93, 125.81, 125.52, 117.34, 114.25, 47.14, 34.55, 31.39, 27.35, 25.84, 22.11 ppm.

Conjugation of 6-{2-(4-Methylpyridin-2-yl)-1*H*-benzo[*d*]imidazol-1-yl}hexanoic Acid with BSA: Complex **4** (1.34×10^{-5} mol), dicyclohexylcarbodiimide (DCC) (2.68×10^{-5} mol) and *N*-hydroxy succinimide (NHS) (2.68×10^{-5} mol) were added to anhydrous DMF (5 mL). The mixture was stirred for 5 h at 70 °C over a silicon oil bath. The total conversion to **4-NHS** was assessed by HPLC using an RP C_{18} column with an acetonitrile/water gradient and UV/Vis detection, and the **4-NHS** was used immediately. *N*-Hydroxysuccinimide ester of **4** (56 μL, 1.50×10^{-7} mol) was added to BSA (1.50×10^{-8} mol) in sodium borate buffer (1 mL, pH 8.5) giving a 10-fold molar excess. After stirring for 2 h at room temperature, *N*-hydroxysuccinimide ester of **4** (56 μL) was added, and the reaction continued for another 2 h. The reaction mixture was then passed over a PD10-type prepacked chromatographic column containing Sephadex G-25 M and was eluted with sodium borate (pH 8.5). One-milliliter fractions were collected and detection was performed at 460 nm. The absorbance and fluorescence spectra of the fractions collected (1–8 mL) showed absorption maxima at 250, 290, 330, and 460 nm with an emission at 630 nm upon irradiation at 460 nm.

Supporting Information Available (see also the footnote on the first page of this article): IR spectra of complexes **1**–**4**.

Acknowledgments

We acknowledge financial support of this work by Regione Piemonte and European Commission DG-XII (IFCA Project, contract number G5RD-CT2002-00723). G.V. and I.M. were supported by the University of Torino and are particularly grateful to Compagnia di San Paolo (Torino) and Fondazione della Cassa di Risparmio di Torino (Italy), for the supply of laboratory equipment. We are indebted to Prof. G. Civera (Politecnico di Torino, Italy) for building a power supply that regulates the amplification of the PMT, and to Prof. D. Viterbo and Dr. G. Croce (Università del Piemonte Orientale, Italy) for useful discussions and assistance during X-ray diffraction analysis. J.B.A.R. gratefully acknowledges support by NSF MCB-0517644 and by NIH COBRE RR-15583.

[1] J. R. Lakowicz, *Principles of Fluorescence Spectroscopy*, Kluwer Academic/Plenum Publishers, New York, **1999**.
[2] U. Kosch, I. Klimant, T. Werner, O. S. Wolfbeis, *Anal. Chem.* **1998**, *70*, 3892–3897.
[3] Z. Murtaza, Q. Chang, G. V. Rao, H. Lin, J. R. Lakowicz, *Anal. Biochem.* **1997**, *247*, 216–222.
[4] C. Krause, T. Werner, C. Huber, I. Klimant, O. S. Wolfbeis, *Anal. Chem.* **1998**, *70*, 3983–3985.
[5] C. Huber, T. Werner, C. Krause, I. Klimant, O. S. Wolfbeis, *Anal. Chim. Acta* **1998**, *364*, 143–151.
[6] G. Neurauter, I. Klimant, O. S. Wolfbeis, *Anal. Chim. Acta* **1999**, *382*, 67–75.
[7] E. Terpetschnig, H. Szmacinski, H. Malak, J. R. Lakowicz, *Biophys. J.* **1995**, *68*, 342–350.
[8] E. Terpetschnig, J. D. Dattelbaum, H. Szmacinski, J. R. Lakowicz, *Anal. Biochem.* **1997**, *251*, 241–245.
[9] H. Szmacinski, E. Terpetschnig, J. R. Lakowicz, *Biophys. Chem.* **1996**, *62*, 109–120.
[10] F. N. Castellano, J. D. Dattelbaum, J. R. Lakowicz, *Anal. Biochem.* **1998**, *255*, 165–170.
[11] A. E. Friedman, J. C. Chambron, J. P. Sauvage, N. J. Turro, J. K. Barton, *J. Am. Chem. Soc.* **1990**, *112*, 4960–4962.
[12] C. Garino, S. Ghiani, R. Gobetto, C. Nervi, L. Salassa, V. Ancarani, P. Neyroz, L. Franklin, J. B. A. Ross, E. Seibert, *Inorg. Chem.* **2005**, *44*, 3875–3879.
[13] C. Garino, R. Gobetto, C. Nervi, L. Salassa, G. Croce, M. Milanesio, E. Rosenberg, J. B. A. Ross, *Eur. J. Inorg. Chem.* **2005**, 606–614.
[14] R. Gobetto, C. Nervi, B. Romanin, L. Salassa, M. Milanesio, G. Croce, *Organometallics* **2003**, *22*, 4012–4019.
[15] M. A. Haga, M. M. Ali, S. Koseki, K. Fujimoto, A. Yoshimura, K. Nozaki, T. Ohno, K. Nakajima, D. J. Stufkens, *Inorg. Chem.* **1996**, *35*, 3335–3347.
[16] D. P. Rillema, D. S. Jones, C. Woods, H. A. Levy, *Inorg. Chem.* **1992**, *31*, 2935–2938.
[17] B. D. J. R. Fennema, R. A. G. Degraaff, R. Hage, J. G. Haasnoot, J. Reedijk, J. G. Vos, *J. Chem. Soc., Dalton Trans.* **1991**, 1043–1049.
[18] N. E. Tokel-Takvoryan, R. E. Hemingway, A. J. Bard, *J. Am. Chem. Soc.* **1973**, *95*, 6582–6589.
[19] N. E. Tokel, A. J. Bard, *J. Am. Chem. Soc.* **1972**, *94*, 2862–2863.
[20] A. Juris, V. Balzani, F. Barigelletti, S. Campagna, P. Belser, A. Von Zelewsky, *Coord. Chem. Rev.* **1988**, *84*, 85–277.
[21] R. S. Nicholson, I. Shain, *Anal. Chem.* **1964**, *36*, 706–723.

[22] In the Stoke–Einstein equation, the diffusion coefficient *D* is inversely proportional to the molecular radius. Assuming a spherical shape, *D* is also inversely proportional to the cubic root of the crystallographic volume of the molecule.
[23] J. O. Bockris, A. K. M. Reddy, *Modern Electrochemistry*, Plenum, New York, **1970**, Chapter IV, p. 380.
[24] C. P. Brock, Y. G. Fu, *Acta Crystallogr., Sect. B: Struct. Sci.* **1997**, *53*, 928–938.
[25] J. V. Casper, J. T. Meyer, *Inorg. Chem.* **1983**, *22*, 2444–2453.
[26] W. J. Miao, J. P. Choi, A. J. Bard, *J. Am. Chem. Soc.* **2002**, *124*, 14478–14485.
[27] M. M. Richter, *Chem. Rev.* **2004**, *104*, 3003–3036.
[28] J. V. Caspar, T. J. Meyer, *J. Am. Chem. Soc.* **1983**, *105*, 5583–5590.
[29] J. Van Houten, R. J. Watts, *J. Am. Chem. Soc.* **1976**, *98*, 4853–4858.
[30] P. McCord, A. J. Bard, *J. Electroanal. Chem.* **1991**, *318*, 91–99.
[31] T. C. Richards, A. J. Bard, *Anal. Chem.* **1995**, *67*, 3140–3147.
[32] F. Barigelletti, L. Decola, V. Balzani, R. Hage, J. G. Haasnoot, J. Reedijk, J. G. Vos, *Inorg. Chem.* **1991**, *30*, 641–645.
[33] H. Z. Zheng, Y. B. Zu, *J. Phys. Chem. B* **2005**, *109*, 12049–12053.
[34] G. T. Hermanson, *Bioconjugate Techniques*, Academic Press, San Diego, CA, **1996**.
[35] X. M. He, D. C. Carter, *Nature* **1992**, *358*, 209–215.
[36] T. Peters Jr, *Adv. Protein Chem.* **1985**, *37*, 161–245.
[37] B. F. Erlanger, *Methods Enzymol.* **1980**, *70*, 85–104.
[38] H. J. Youn, E. Terpetschnig, H. Szmacinski, J. R. Lakowicz, *Anal. Biochem.* **1995**, *232*, 24–30.
[39] E. Terpetschnig, H. Szmacinski, J. R. Lakowicz, *Anal. Biochem.* **1995**, *227*, 140–147.
[40] M. M. Bradford, *Anal. Biochem.* **1976**, *72*, 248–254.
[41] L. F. Amarengo, D. D. Perrin, *Purification of Laboratory Chemicals*, Butterworth-Heinemann, Oxford, **1998**.
[42] B. P. Sullivan, D. J. Salmon, J. T. Meyer, *Inorg. Chem.* **1978**, *17*, 3334–3341.
[43] S. Hiiromitsu, K. Takeo, H. Takeru, *J. Pharm. Sci.* **1988**, *77*, 855–860.
[44] E. Barni, P. Savarino, *J. Heterocycl. Chem.* **1977**, *14*, 937–940.
[45] E. Barni, C. Barolo, P. Quagliotto, P. Savarino, G. Viscardi, D. Marabello, *J. Heterocycl. Chem.* **2003**, *40*, 649–654.
[46] SMART© 1998, Madison, WI 53719, USA, Bruker AXS, Inc., **1998**.
[47] G. M. Sheldrick, *SADABS*, Germany, University of Göttingen, **1996**.
[48] A. Altomare, M. C. Burla, M. Camalli, G. L. Cascarano, C. Giacovazzo, A. Guagliardi, A. G. Moliterni, G. Polidori, R. Spagna, *J. Appl. Crystallogr.* **1999**, *32*, 115–119.
[49] G. M. Sheldrick, *SHELXL-97*, University of Göttingen, Germany, **1997**.
[50] *SHELXTL*, Bruker AXS, Inc., Madison, WI 53719, USA, **1998**.

Received: February 3, 2006
Published Online: May 29, 2006

